MAY 21 2025

Underwater soundscape and vector acoustic observations during a seismic airgun survey near coastal Oregon

Katherine R. Heal ; Kaustubha Raghukumar

J. Acoust. Soc. Am. 157, 3848–3859 (2025)
https://doi.org/10.1121/10.0036728

JASA ARTICLE

Underwater soundscape and vector acoustic observations during a seismic airgun survey near coastal Oregon

Katherine R. Heal[1] and Kaustubha Raghukumar[2,a)]
[1]Biological Sciences Division, Pacific Northwest National Laboratories, Richland, Washington 99352, USA
[2]Integral Consulting Inc., Santa Cruz, California 95062, USA

ABSTRACT:
In the summer of 2021, a seismic survey occurred near Southern Oregon to map the Cascadia Subduction Zone using an array of airguns. To evaluate the effect of the survey on the soundscape within a marine protected area, acoustic measurements were conducted using a vector sensor array deployed in 36 m deep water. Resulting data were analyzed using acoustic metrics, some of which are commonly used in soundscape studies, while others are gaining popularity in ecological acoustics. While cumulative sound exposure levels were dominated by wind noise, other metrics such as peak sound pressure, kurtosis, Acoustic Complexity Index, and crest factor, showed clear signals associated with the seismic survey. Further, when the seismic survey vessel was closest to the measurement location, a good correlation was observed between sound pressure (peak and root mean squared) and sound exposure levels computed using sound pressure versus those computed using particle velocity. At lower signal-to-noise ratios, or in the absence of seismic pulses, velocity-based acoustic metrics showed considerable contamination by flow and other noise. Our analysis suggests that pressure measurements alone may be sufficient (and even preferable) for evaluating organismal particle velocity dosage, whenever the signals of interest have sufficient signal-to-noise ratio.
 https://doi.org/10.1121/10.0036728
(Received 18 November 2024; revised 29 April 2025; accepted 30 April 2025; published online 21 May 2025)
[Editor: Aaron M. Thode] Pages: 3848–3859

I. INTRODUCTION

Seismic surveys to collect geophysical data of the seafloor using airgun pulses produce intense sound pulses that can potentially affect marine animals. The effect of these airgun pulses on marine mammals has been a subject of research for decades and has led to guidelines to mitigate the effect that intense noise sources can have on marine mammals and sea turtles. Although less research has been done on fishes and invertebrates, anthropogenic sound can also injure, cause behavioral changes, or mask communication among these species (e.g., Casper *et al.*, 2013; Halvorsen *et al.*, 2012).

Unlike marine mammals that sense the pressure component of sound, fishes and marine invertebrates primarily use the particle motion component of sound to acquire information within their environment (Popper and Hawkins, 2018). Most studies on sound in both open oceans and shallow-water environments have focused on sound pressure, and investigations of the soundscape and potential impact of sound on fishes and invertebrates have often overlooked the sensitivity of many of these animals to the particle motion that accompanies the transmission of the sound. As a result, there are not yet any specific regulatory exceedance thresholds for acoustic particle motion. While acoustic particle motion can be generally inferred from pressure in a spatially homogenous field, the relationship was thought to be complicated in the near field and close to reflecting boundaries (Gray *et al.*, 2016; Nedelec *et al.*, 2016). As a result, vector sensors have been employed to measure the particle motion component of sound to directly collect velocity measurements (e.g., Jones *et al.*, 2022). More recently, time-averaged particle velocity metrics have been shown to be easily inferable from acoustic pressure measurements (Dahl *et al.*, 2024; Flamant and Bonnel, 2023), even near boundaries, lessening the need for specific particle velocity measurements for kinematic dosage studies.

A seismic survey of the Cascadia Subduction Zone occurred offshore of Oregon, Washington, and British Columbia during the summer of 2021 using an array of 36 airguns over the course of 40 days. During this airgun activity, the soundscape was monitored within the Redfish Rocks Marine Reserve (RRMR) near Port Orford, Oregon, using a vector sensor array (VSA) to simultaneously measure the particle motion and pressure components of sound. The RRMR supports a wide diversity of fish and invertebrates within its rocky reefs, kelp beds, and emergent rocks. Virtually all studies of airgun survey sound impacts in both open ocean and shallow-water environments focus solely on the pressure component of sound propagation (e.g., Gordon *et al.*, 2003; McCauley *et al.*, 2003; Richardson *et al.*, 1986), but few focus on the particle motion that accompanies the transmission of the sound to which all fish (Fay, 1984) and some invertebrates (Mooney *et al.*, 2012) have sensitivity. The acoustic pressure and particle velocity data obtained are described using a variety of metrics. In addition to the more common metrics, such as root mean square (rms) sound pressure level, peak sound

a)Email: kraghukumar@integral-corp.com

https://doi.org/10.1121/10.0036728

pressure level (SPL_{pk}), sound exposure level (SEL) and kurtosis—two bioacoustic metrics [Acoustic Complexity Index and crest factor (CF)] that have their origin in terrestrial acoustics (Bohnenstiehl *et al.*, 2018) are also investigated. The higher-order bioacoustic metrics are finding increasing use in underwater soundscape studies due to their ability to describe the overall structure of an acoustic environment in terms of the time-frequency intensity distribution and complexity created by an ensemble of acoustic signals and their ecological relevance (Pegg *et al.*, 2021; Mattmüller *et al.*, 2024). While the use of these metrics has had mixed results in underwater soundscape studies, they have been presented for two reasons: (1) as soundscapes are often influenced by biological sounds, it is important to characterize them in terms of metrics that capture ecological richness; and, (2) as particle velocity effects on fishes and invertebrates draw increased attention (Nedelec *et al.*, 2016), it is thought important to express these metrics not only in terms of pressure, but also in terms of particle velocity. While no claims are made on the effects of noise on marine life with relation to these metrics, the goal is to shed light on the variability of these metrics with regard to the airgun survey in both pressure and velocity space.

The overall objectives of this study are to (1) describe the effect that the seismic survey had on the soundscape within the RRMR using a variety of pressure and velocity-based acoustic metrics, (2) simultaneously measure the particle motion and pressure components of the seismic survey activity, and (3) develop an understanding of the predictability between particle motion and sound exposure metrics that are relevant to the protection of marine fish and invertebrate resources.

II. APPROACH

A. Equipment and deployment

Measurements of acoustic pressure and particle velocity were made using a three-element acoustic VSA, which was deployed in approximately 36 m–deep water at 42° 41' 44.052'' *N*, 124° 28' 47.028'' *W* within the RRMR on May 15, 2021, and recovered on July 21, 2021. Two equipment turnarounds occurred within this deployment period on June 8 and June 30, 2021. For the purposes of analysis, the three deployment periods are categorized as "pre-survey" (May 18–29), "during" (June 8–16), and "post-survey" (July 3–11). During each deployment period, 11 days of continuous acoustic data were gathered.

The VSA, NoiseSpotter® (Integral Consulting Inc., Santa Cruz, CA) (Raghukumar *et al.*, 2020) (Fig. 1), consists of a fiberglass bottom platform with multiple high density polyethylene (HDPE) rods that make up a three-dimensional structure. Mounted on the HDPE structure are three sensors at heights of 35, 50, and 75 cm above the seabed. Sensors were separated by 1 m in the horizontal. Particle motion measurements are comprised of three-dimensional particle velocity vectors (u, v, w) that are translated into a true earth-referenced frame using auxiliary measurements from an integrated inertial motion unit (IMU). The acoustic vector sensors are sensitive to acoustic frequencies in the 50 Hz to 3 kHz range and are sampled at 20 kHz using a single clock for all three sensors. Data from the sensor 50 cm above the seabed was of poor quality due to a faulty connector, while the data on the sensor 75 cm above the seabed showed a higher degree of contamination by flow noise as discussed subsequently. Consequently, most analysis in this study is applied to data from the sensor 35 cm above the seabed.

To facilitate quality data acquisition in energetic environments, the VSA included flow noise suppression shields around each vector sensor. The flow noise suppression shields have been demonstrated to be effective in reducing flow noise effects, thereby improving data quality and signal detectability (Raghukumar *et al.*, 2019).

B. Seismic survey

The *R/V Langseth* conducted a seismic airgun survey of the Cascadia subduction zone from May 31 to July 11, 2021, as part of the CAsie Seismic Imaging Experiment (CASIE21) (Carbotte *et al.*, 2024). The survey commenced near Seattle, proceeded southward until near the Oregon–California border on June 17, 2021, and then continued northward until offshore of British Columbia on July 8, 2021 before concluding the survey on July 11, 2021 (Fig. 2). The second VSA deployment (June 8–19, 2021) was timed to coincide with these close distances during which airgun volumes were in the range 4230–5160 cm^3, highlighted in red in Fig. 2, and labeled as "during" in this work. On June 11, 2021, the day of the closest point of approach, airgun volumes were between 4980 and 5160 cm^3 every 17–30 s. The final VSA deployment (July 3–11, 2021) coincided with times where the *R/V Langseth* was off the coast of Washington and over 400 km away from RRMR (highlighted in red in Fig. 2). Due to the distance, the seismic survey is unlikely to have any effect on the soundscape of the RRMR during this period; therefore, we refer to this as the "post-survey" period in this work.

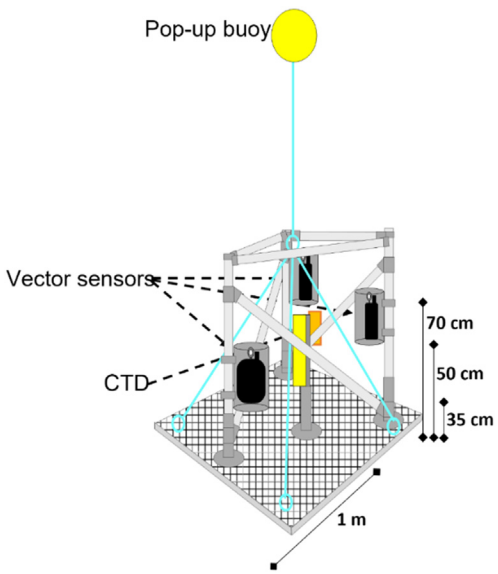

FIG. 1. Schematic of NoiseSpotter VSA. CTD, conductivity-temperature-depth sensor.

C. Meteorological data

To investigate the effect of seismic pulses within the ambient soundscape, data associated with other noise sources, including wind and wave data, were collated. The wind data were measured at the National Data Buoy Center station Port Orford meteorological station, located on a dock located roughly 3 km north of the sensor array [Fig. 2(B)]. This specific meteorological station does not record wave data. Wave data were used from National Data Buoy Center 46 015 meteorological buoy, which is located approximately 30 km offshore of the VSA. Due to the distance of the buoy with wave data compared to the sensor array, we limit our interpretation to only giving broad context to the wave activity in the area, not specifically applicable to the RRMR.

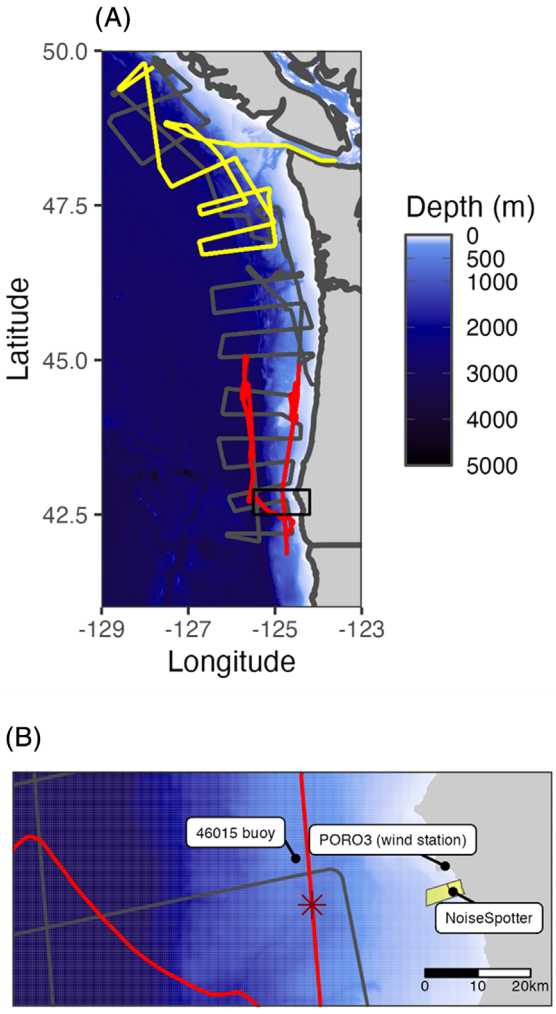

FIG. 2. (A) Full track of *R/V Langseth* during seismic survey off the northwest coast of the United States. Highlighted on the track are the times with NoiseSpotter data, corresponding to the "during" and "post-survey" periods in red and yellow, respectively. (B) Inset [as boxed in (A)] of RRMR (in yellow), VSA and meteorological sensor locations, and *R/V Langseth* track highlighted as in (A). Starred is the point where the of *R/V Langseth* was nearest to the NoiseSpotter during data acquisition (27 km distance on June 11, 2021 at 2 AM local time). Bathymetric data were acquired from Earth TOPOgraphy 1-arc second database hosted by National Oceania and Atmospheric Administration (Amante and Eakins, 2009) using the marmap package in *R* (Pante and Simon-Bouhet, 2013).

D. Calibration and initial data processing of acoustic data

Initial data processing of the vector sensor data consisted of applying manufacturer-provided sensor-specific calibration curves to transform voltage time series to pressure and velocity time series in units of micro-Pascal and meters/s, respectively. Acoustic pressure and particle velocity time series data were Hanning-windowed and calibrated in the frequency-domain using the calibration curves, and then Fourier-transformed back into the time-domain. Phase offsets between the pressure and velocity channels were also corrected using sensor-specific phase calibration curves. The pressure sensitivity of the sensors is flat in the 50 Hz to 3 kHz frequency range, while the velocity sensitivity peaks at 1 kHz with an approximately 23 dB/decade roll-off in sensitivity on either side of the 1 kHz peak. All pressure and particle velocity time series are bandpass filtered in the 50–3000 Hz frequency band to remove any direct current offsets and to limit the frequency content to that which the vector sensors are most sensitive to.

E. Isolating periods of flow noise

Previous work has shown that particle velocity measurements are suspect to flow noise (Raghukumar *et al.*, 2019; Thode *et al.*, 2021). To isolate times of flow noise, kinetic to potential energy (K/P) [Eq. (1)] was used as a diagnostic, as described in Thode *et al.* (2021),

$$\frac{K}{P} = \frac{\frac{1}{2}\rho_0 \left\langle \left(v_x^2 + v_y^2 + v_z^2 \right) \right\rangle}{\left(\frac{1}{2\rho_0 c^2} \right) \langle p^2 \rangle}, \tag{1}$$

where ρ_0 is the density of seawater; c is the sound of speed in seawater; v_x, v_y, and v_z are the particle velocities in the x, y, and z directions, respectively; and p is the pressure. On average, K/P $\simeq 1$ within instrument calibration error; K/P > 1 generally indicates non-acoustic contamination, such as by flow noise. An exception to this occurs when there is a coherent broadband source directly above the sensor (Dahl and Dall'Osto, 2022) in which case K/P oscillates between being >1 in some frequency bands while being <1 in neighboring frequency bands. However, for non-vertical sources, including diffuse sources, such as ambient noise, K/P should average to ~ 1. While more sophisticated methods exist to quantify non-acoustic contamination (D'Spain *et al.*, 1991), the first-order method of filtering data that has a K/P ratio much greater than 1 was used, like that used by Thode *et al.* (2021).

K/P was calculated on spectrograms and originally sampled time series. By visualizing K/P over individual spectrograms, it was recognized that the highest contribution of flow noise was in the lower frequency data (<300 Hz) (see Fig. 3). Therefore, a bandpass filter was applied to isolate the 50–100 Hz range in the originally sampled data and flagged times where the 0.1 s rolling median of K/P exceeded 1.

F. Identifying periods of seismic airgun activity

To examine the acute effects of the seismic airgun survey on the sound field in the RRMR, the entire acoustic

https://doi.org/10.1121/10.0036728

dataset was searched to detect times with seismic survey pulse sequences, generally following the approach outlined in Martin (2013). Figure 3 shows a typical 1-min spectrogram with detected airgun pulses marked.

First, 300 s–long spectrograms were created with a 4.88 Hz frequency resolution and 0.2 s time resolution [4096 point fast Fourier transform (FFT); 90% overlap] and used to subset the spectrogram for the 100–1000 Hz frequency range. Each frequency bin was normalized over the 300 s window and contours were identified within the spectrogram that exceeded three times this median. Contours that spanned at least 60 Hz and were between 0.2 and 6 s in duration were retained; all others were removed. Next, an "event" time series was created by summing the median-normalized values in each time bin that contained non-removed contours and auto-correlated this event time series, smoothed the resulting autocorrelation using a Satizky–Golay filter with a window length of 3. The first period maxima that was between 4.8 and 60 s with a correlation of greater than 0.1 was then extracted. The original time series data were then searched for peaks that matched this periodicity and any peaks that did not correspond to peaks in the event time series were removed. To reduce false positives, peaks were excluded that lasted longer than 3 s at 90% peak intensity. Additionally, peaks were removed that did not occur within a series of at least 20 other peaks, with a time gap of 10–60 s between each pulse.

G. Calculation of metrics

Several metrics were calculated to characterize the soundscape, to explore the effect that the seismic pulses had on the soundscape, and to develop an understanding between the pressure and velocity components of underwater sound in this important ecosystem. Unless otherwise stated, all metrics were calculated on originally sampled data after applying a bandpass filter to isolate 50–3000 Hz to allow for direct comparisons of the pressure and velocity components. The metrics calculated were sound pressure level (SPL), SPL_{pk}, SEL, kurtosis, CF, and Acoustic Complexity Index (ACI)—all described in detail below.

Each one of the metrics described in this section can be calculated for the pressure component (as is typical) and for the magnitude of particle velocity component (less typical), wherein any pressure measurements and intensities are replaced with particle velocity magnitudes and intensities. Particle velocity magnitude is calculated by combining the individual vector components according to Eq. (2),

$$v = \sqrt{\left(v_x^2 + v_y^2 + v_z^2\right)}. \tag{2}$$

For metrics that were calculated for both velocity and pressure components, a velocity counterpart is defined and calculated after removing times with detected flow noise. In each of the metrics, p_0 is 1 μPa and for particle velocity, v_0 is 1 nms^{-1}.

1. SPL and sound velocity level (SVL)

SPL is the root mean squared (RMS) pressure level in a stated frequency band over a specified time window, expressed in dB re 1 μPa for pressure. Its velocity counterpart is SVL, expressed in dB re 1 nms^{-1}. In this work, SPL and SVL refer to an RMS pressure or velocity level and are not instantaneous. Given a measurement of the time varying sound pressure, $p(t)$, or particle velocity, $v(t)$, from a given noise source, the SPL or SVL is computed according to Eqs. (3) and (4) where $p(t)$ is the pressure as a function of time and $v(t)$ is total particle

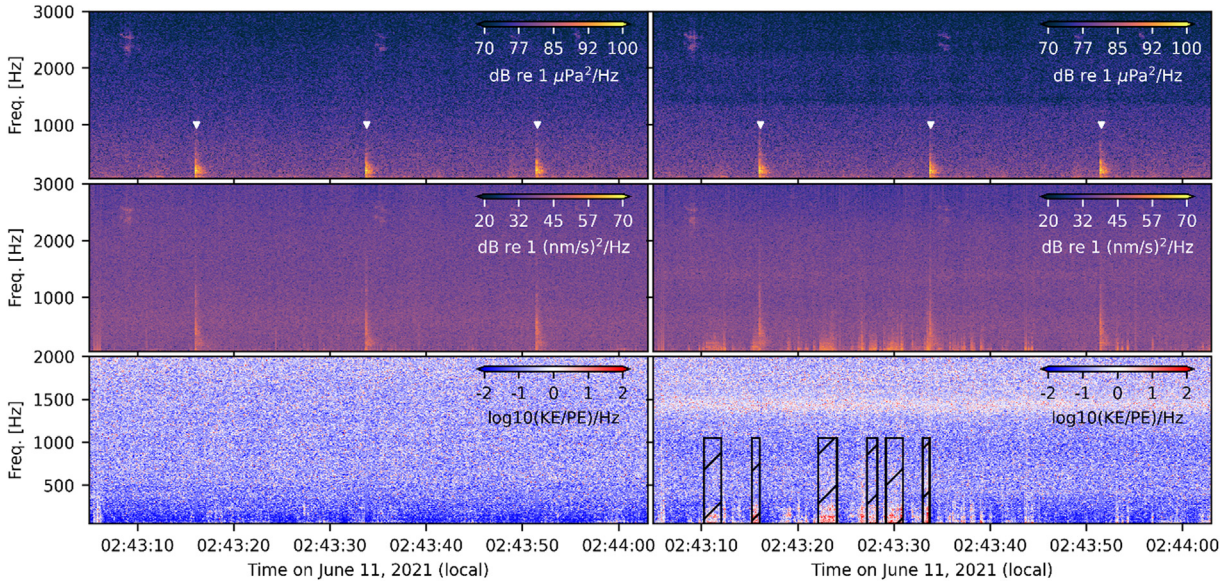

FIG. 3. Spectrograms for both the 35 cm sensor (left column) and the 70 cm sensor (right column). For both sensors, the top row is pressure, middle row is velocity, and bottom row is K/P. Detected seismic pulses are marked in the top row with inverted triangles (frequency is arbitrary; the detection is in the time dimension only). Times with significant flow noise are marked in K/P spectrograms as hashed areas (again, arbitrary frequency domain; time detection only). There was no appreciable flow noise detected in the 35 cm sensor over this time period. Freq., frequency.

velocity measured over the pulse duration $0 \leq t \leq T$. A pulse duration of 1 min is used in the analysis,

$$SPL = 10\log_{10}\left(\frac{1}{T}\int_T p^2(t)dt/p_0^2\right), \tag{3}$$

$$SVL = 10\log_{10}\left(\frac{1}{T}\int_T v^2(t)dt/v_0^2\right). \tag{4}$$

2. SPL_{pk} and peak sound velocity level (SVL_{pk})

SPL_{pk} is the maximum noise level over a given event and is calculated using the maximum variation of the pressure from positive to zero within the wave, expressed in dB re 1 μPa. Its velocity counterpart is SVL_{pk}, expressed in dB re 1 nms^{-1}. The peak level is used as a descriptor for impulsive sound source. SPL_{pk} or SVL_{pk} are computed according to Eqs. (5) and (6).

$$SPL_{pk} = 10\log_{10}\left[\frac{\max\left(\left|p^2(t)\right|\right)}{p_0^2}\right] \tag{5}$$

$$SVL_{pk} = 10\log_{10}\left[\frac{\max\left(\left|v^2(t)\right|\right)}{v_0^2}\right] \tag{6}$$

3. SEL and its velocity counterpart (SEL_V)

SEL is similar to SPL but further specifies the sound pressure over a specified time interval or event, for a specified frequency range, expressed in dB re 1 μPa^2s. Its velocity counterpart is SEL_v and is expressed in dB re 1 nm^2s^{-1}. SEL and SEL_v can be computed for both long- and short-time scales according to Eqs. (7) and (8), so reporting the time length is essential to aid in understanding of the value of the metric. Both hourly and minute SELs and SEL_v are computed in this study, as specified. Often, particularly for regulatory applications, 24-h SELs are computed, and denoted by the symbol, $L_{E,24}$. Here, the use of the symbol SEL for a calculation for other lengths of time is used to distinguish from the 24 h calculation. In Eqs. (7) and (8), T_0 is a reference time interval of 1 s,

$$SEL = 10\log_{10}\left(\int_0^T p^2(t)dt/T_0p_0^2\right), \tag{7}$$

$$SEL_v = 10\log_{10}\left(\int_0^T v^2(t)dt/T_0v_0^2\right). \tag{8}$$

4. Kurtosis and $kurtosis_v$

Kurtosis is a unitless metric of impulsivity within a soundscape that describes the tailedness of the probability distribution of a random variable. For a time series of pressure, $p(t)$, kurtosis is defined in Eq. (9), where $\overline{p}$ is the mean pressure over a time period from t_1 to t_2. This metric is described and evaluated for underwater soundscape descriptions in Wilford *et al.* (2021). Values higher than 40 are generally considered impulsive, and Gaussian-distributed random noise produces values of 3. Kurtosis is computed over 1 min periods in this study,

$$Kurtosis = \frac{\mu_4}{\mu_2^2}, \tag{9}$$

$$\mu_2 = \frac{1}{t_2 - t_1}\int_{t_1}^{t_2}[p(t) - \overline{p}]^2dt, \tag{9a}$$

$$\mu_4 = \frac{1}{t_2 - t_1}\int_{t_1}^{t_2}[p(t) - \overline{p}]^4dt. \tag{9b}$$

The velocity counterpart for kurtosis is $kurtosis_v$, described in Eq. (10), where $\overline{v}$ is the mean velocity magnitude.

$$Kurtosis_v = \frac{\mu_{v4}}{\mu_{v2}^2} \tag{10}$$

$$\mu_{v2} = \frac{1}{t_2 - t_1}\int_{t_1}^{t_2}[v(t) - \overline{v}]^2dt \tag{10a}$$

$$\mu_{v4} = \frac{1}{t_2 - t_1}\int_{t_1}^{t_2}[v(t) - \overline{v}]^4dt \tag{10b}$$

5. CF and particle velocity counterpart (CF_v)

CF is a second measure of impulsivity, defined as the difference between the SPL_{pk} and SPL (in dB re 1 μPa) [Eq. (11)]. CF_v is the particle velocity counterpart of CF, defined as the difference between the SVL_{pk} and SVL (in dB re 1 nms^{-1}) [Eq. (12)]. A CF of 1 indicates no peak, and larger CF values correspond to larger diversions of impulsive sounds within the soundscape. CF is a non-statistical measure that focuses on peak values, while kurtosis is a statistical measure that assesses the presence and extent of outliers or "tailedness" in a signal,

$$CF = SPL_{pk} - SPL, \tag{11}$$

$$CF_v = SVL_{pk} - SVL. \tag{12}$$

6. Acoustic Complexity Index (ACI) and its particle velocity counterpart (ACI_v)

ACI was developed in terrestrial environments to estimate the complexity of an acoustic recording in space and time (Farina and Morri, 2008; Pieretti *et al.*, 2011). Although its use and interpretability are still under discussion within the underwater soundscape, ACI has been shown to increase in the presence of broadband impulsive signals (Bohnenstiehl *et al.*, 2018). In a spectrogram of n non-overlapping time steps and m non-overlapping frequency bins, to calculate ACI, the absolute difference in intensity (I) between adjacent time steps (k) along each frequency bin (i) is first calculated. These differences are then summed and normalized by the sum of intensity within each frequency bin. The final ACI value is the sum of these values across all

https://doi.org/10.1121/10.0036728

frequency bins. Equation (13) shows the full calculation. ACI_v is the particle velocity counterpart of ACI, calculated on the spectrogram of particle velocity, shown in Eq. (14). Note that the length of the segment, the number of points used in calculating the FFT, and original sampling rate of the data, all influence the time and frequency resolution and need to be consistent to enable comparisons for this unitless metric,

$$ACI = \sum_{i=1}^{m} \frac{\sum_{k=1}^{n} |I_{ik} - I_{ik}|}{\sum_{k=1}^{n} I_{ik}}, \tag{13}$$

$$ACI_v = \sum_{i=1}^{m} \frac{\sum_{k=1}^{n} |I_{ik} - I_{ik}|}{\sum_{k=1}^{n} I_{ik}}. \tag{14}$$

H. Statistical approaches

To evaluate the effect that the seismic airgun pulse had on the soundscape within the RRMR, a variety of multivariate and univariate tests were applied on each of the metrics described above. First, dataset was downsampled fivefold for statistical analyses. Next, a principal component analysis (PCA) was performed to visualize the multivariate space based on either the pressure or velocity metrics. PCA was performed on standardized (centered and scaled with mean of zero and standard deviation of one) metrics and thus, the resulting principal components (PCs) are unitless. The results of the airgun-pulse detection method was applied and used to label each sample with presence/absence of seismic airgun pulse detected. With these labeled data, a multivariate permanova (McArdle and Anderson, 2001) was applied to test whether the samples were significantly different in the tested multivariate space (pressure or velocity metrics) with 99 permutations. Univariate tests were also applied on each metric separately using a *t*-test and an approximate one-way Fisher–Pitman permutation test with 9999 permutations. All statistics were performed in *R* v4.3.1 (R Foundation for Statisitical Computing, Vienna, Austria) using base (*t*-test), vegan (v2.6, Oksanen *et al.*, 2025), and coin (v1.4-3, Hothorn *et al.*, 2006) packages.

To investigate the correlation between velocity and pressure-based metrics of the same variety, a Pearsons correlation was applied and used to obtain a confidence interval for the correlation coefficient by bootstrapping, and a *p*-value by randomization.

III. RESULTS AND DISCUSSION

A. Overview of survey

As mentioned earlier, the three deployment periods are categorized as "pre-survey" (May 18–29, 2021), "during" (June 8–16, 2021), and "post-survey" (July 3–11, 2021; at which point the *R/V Langseth* was over 400 km away from RRMR).

There is a clear diel pattern in wind in both the "pre-survey" and "post-survey" periods with the highest wind speeds observed generally in the afternoon/evening and low wind speeds in the early hours of each day (Fig. 4). Higher sustained wind speeds were observed during the post-survey period. The during period has some diel patterns in wind and hourly SEL during the early and later part of the period, but from June 10–12, 2021, the winds are dominated by strong southerly winds from local storm activity that did not die down over the evening of June 11, 2021. This time also corresponds to increased significant wave height offshore and higher than average SEL. The pattern in SEL largely mirrors wind speeds during all three deployment periods, corroborating previous work that showed a dominance of SEL by wind noise (Haxel *et al.*, 2019). The largest SELs were observed during the stormy period spanning June 10–12, 2021, which is also when the *R/V Langseth* was at its closest point of approach, making it potentially difficult to tease out the contribution to the soundscape from the seismic surveys from SEL observations alone. Finally, higher average SELs during the post-survey period were observed, in line with higher sustained wind speeds during this period. While boat traffic was occasionally observed when visually inspecting spectrograms, boat noise was not specifically analyzed due to their sparse presence in the marine reserve.

B. Characterizing the effects of seismic airgun pulses in a coastal system and soundscape metrics

Using the seismic airgun pulse detection technique, largely adapted from Martin (2013), seismic airgun pulses were detected from June 10–11, 2021. During this time, the *R/V Langseth* was 44 km away from the NoiseSpotter.

A total of 1444 individual airgun pulses were detected from June 10 at 23:11 until June 11 at 07:00 (local time), with a maximum SPL_{pk} of 165 dB re 1 μPa. The seismic airgun pulses had noticeable effects on all calculated metrics computed from acoustic pressure at the sensor located 35 cm above the sea floor (Fig. 5). Over the entire dataset, the highest observed SPL, SPL_{pk}, kurtosis, CF, and ACI (binned over 1 min increments) were observed concurrently with the airgun pulses (Fig. 5). A PCA was used to visualize the relationships between different minutes of acoustic data based on pressure metrics by reducing the pressure-based metrics into combined PCs (Fig. 6). In this multivariate space based on pressure metrics, times with detected airgun pulses were significantly different than those from times without detected airgun pulses (permanova p-value < 0.01) (Fig. 6). All pressure metrics were significantly different in times with detected airgun pulses in both *t*-tests and one-way permutation tests (Table I).

The metrics, when applied to pressure measurements, all show significant deviations when the seismic surveys are present (Figs. 5 and 6; Table I). However, while metrics such as SPL and SPL_{pk} also show the contribution of wind-generated noise, this contribution is almost completely filtered out in the kurtosis metric, which is particularly applicable to distinguish the contribution of impulsive signals (Fig. 5). The CF also appears to capture the impulsivity

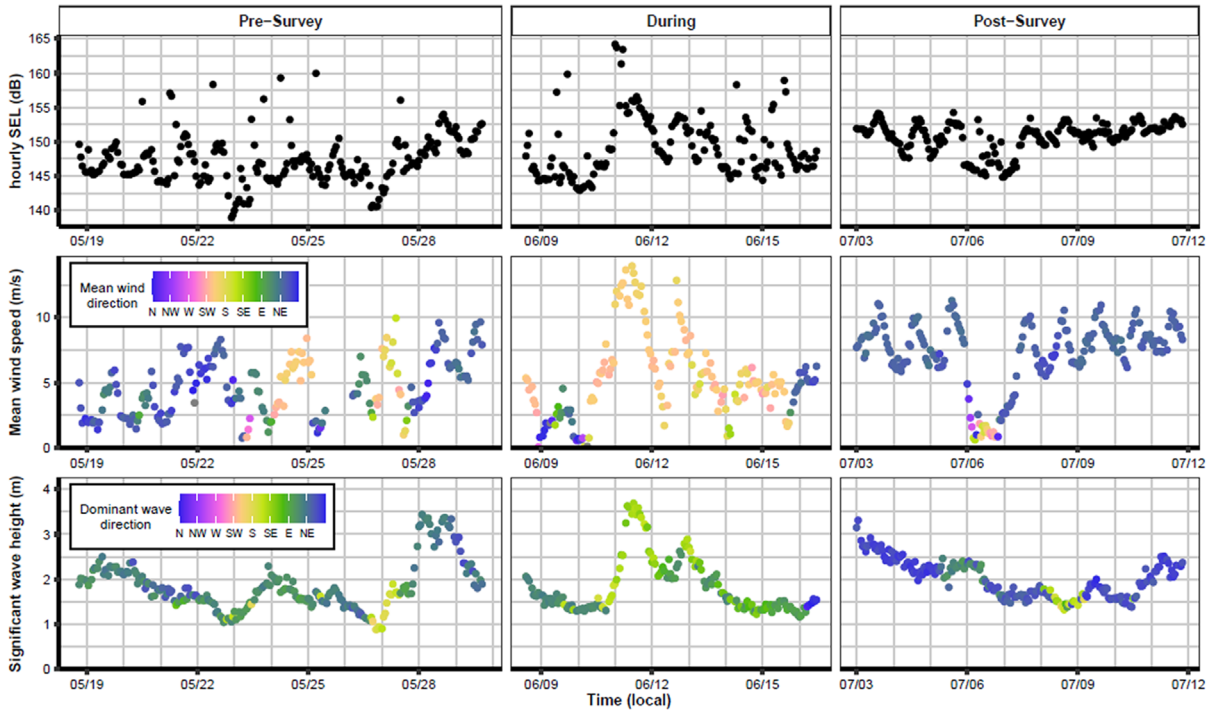

FIG. 4. Long-term patterns in SEL, wind, and waves over the course of the VSA deployment at RRMR. Note that the wave data are from 30 km offshore and should not be interpreted as local RRMR wave conditions. Hourly SEL (pressure, bandpass filtered 50–3000 Hz) for sensor 35 cm above sea floor (top row), as well as mean wind speed (middle row), and significant wave height (bottom row).

of the seismic pulses, while removing the day-to-day variability in wind-generated sound (Fig. 5). The ecosystem metric, ACI, on the other hand, appears to be artificially skewed by the presence of impulsive sound (Fig. 5), which is unsurprising given that it is calculated using frequency and time-differentiation. Outside of the period of seismic noise, however, a rich signal appears to be present that does not appear to be contaminated by wind noise, evidenced by the lack of a consistent diurnal pattern in ACI, unlike SPLs or SELs. For example, periods of elevated ACI (May 20, 2021 or July 6, 2021), do not appear to be highly influenced by wind noise. After July 7, 2021, however, when there are sustained high winds, ACI appears to settle to low levels with little variability, likely due to sustained wind noise with little temporal or frequency variability (Fig. 5).

In general, the same metrics when applied to particle velocity (Fig. 7) appear to have a higher variance between the 20th and 80th percentiles levels over the 30 min analysis windows, indicating that the particle velocity measurements are particularly sensitive to ambient noise. The data shown in Fig. 7 have been masked to remove periods of sustained flow noise as described, and therefore appear to reflect actual acoustic noise, and not flow noise, which represents non-acoustic pressure fluctuations. Unfortunately, this masking precludes displaying SEL_v in a time series as this metric is integrated over time, so while we can use this metric to investigate how well it correlates to SEL by using the same time masking on both metrics, we cannot use it to compare to the other metrics, which are not dependent on a time integration. While all the velocity-based metrics investigated over the time series showed some perturbation during the seismic airgun survey, the velocity metrics do not appear to offer as clear an insight into the presence of impulsive sounds (Fig. 7). This is recapitulated in the univariate tests where only SVL, SVL_{pk}, and CF_v showed significant differences in one-way permutation tests between times with and without detected airgun pulses, and the *p*-values of the velocity metrics were larger (less statistically significant) than their pressure counterparts (Table I). This is likely due to contributions from wind and wave-generated noise, which appear to have more of an effect on particle velocity than pressure. For example, while the SVL values show a distinct peak in the morning of June 11, 2021, this is overshadowed by higher SVL values later in the day when both wind speeds and wave heights are increased (Figs. 4 and 7). This overshadowing is significantly more pronounced on particle velocity than pressure (where the highest SPL is observed during the seismic airgun survey), further indicating that the particle velocity channels of the sensors are highly sensitive to contamination by ambient acoustic noise.

C. Considerations in using vector sensors

Vector sensors offer opportunities for scientists to investigate aspects of the acoustic environment, such as localization (Thode *et al.*, 2010) and polarization (Bonnel *et al.*, 2021), as well as metrics based on the velocity magnitude like those presented here. In our study, we found that considerable amount of the velocity data were affected by flow noise (Fig. 8), particularly in the during and post-survey periods, likely related to higher wind or wave action during these times. The flow noise contamination occurred despite the presence of a flow shield, indicating that while the shield has

https://doi.org/10.1121/10.0036728

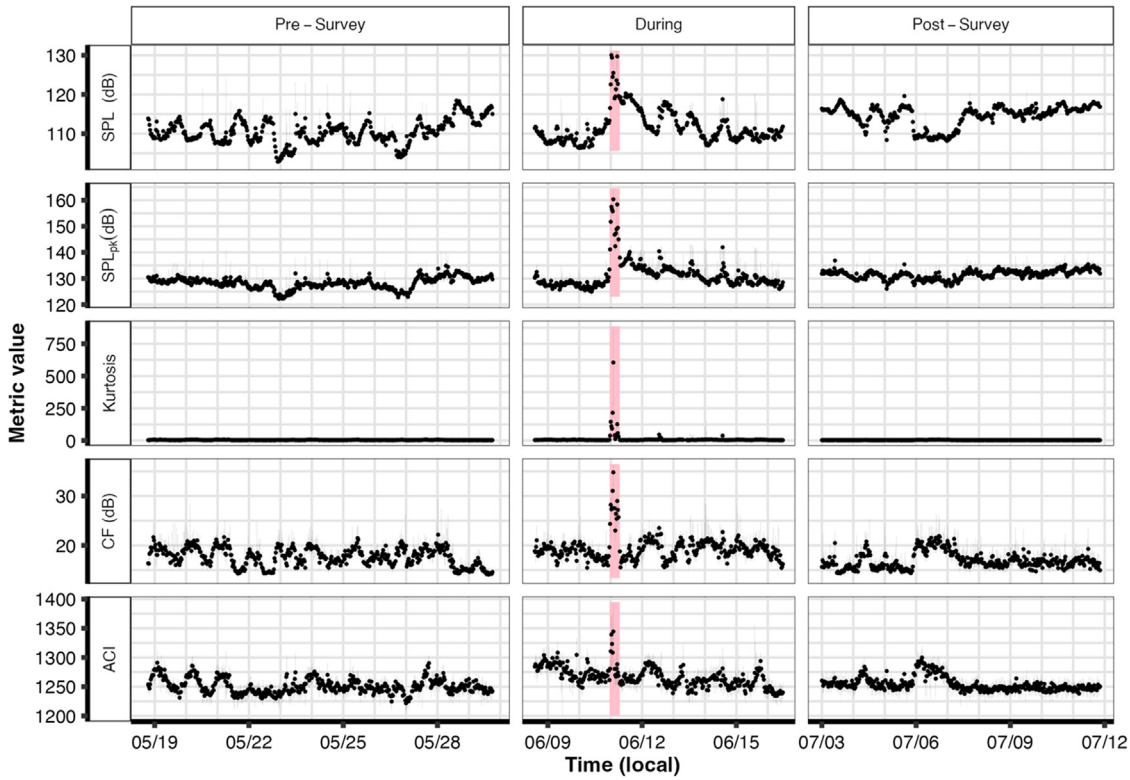

FIG. 5. Time series of soundscape metrics for pressure sensor 35 cm above sea floor (bandpass filtered 50–3000 Hz). Metrics were calculated for every minute of data; each marker is median of 30 min, with the 20th–80th percentiles of data shown in bars. Time period where seismic pulses were detected are highlighted in the during period.

some effectiveness (Raghukumar *et al.*, 2019), there are limitations in stronger flows. Interestingly, the sensor closer to the sea floor was marginally more susceptible to flow noise in the pre-survey period, while the opposite is true during the post-survey period. Since wave and wind-generated velocities generally decay in strength closer to the sea floor, it is expected that a sensor higher in the water column would experience more flow noise. Tidal oscillations were highest during the pre-survey period, and it is possible that the sensor close to the seafloor experienced somewhat stronger tidal currents.

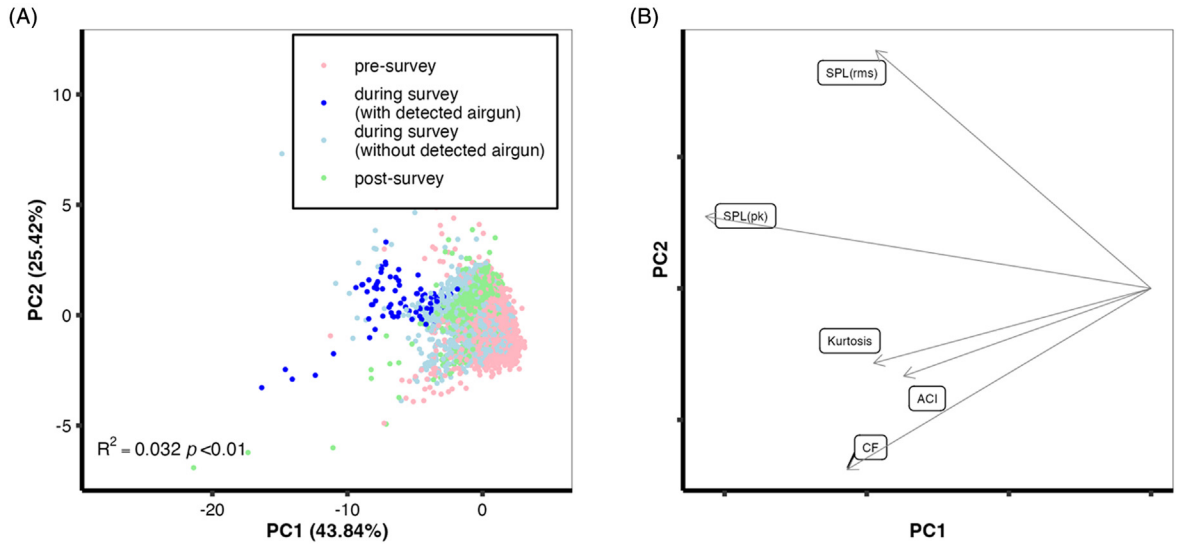

FIG. 6. PCA results of pressure metrics displaying the relationships between (A) samples and (B) variables (a unitless display to show direction only). On (A), points on the plot represent individual 1 min segments of data, with their relative positions indicating how similar each 1 min segment of data are to each other, based on calculated and standardized pressure metrics. Results from permanova test between times with and without detected airgun pulses and percent of variability explained by first two PCs are reported on (A). (B) Shows how each metric contributes to each principal component mapped in (A). Note that samples have been downsampled to 1 min/5 min increment for visualization purposes and SEL was not included because for 1 min increments it covaries with SPL.

TABLE I. Summary statistics for univariate tests for a variety of pressure and velocity-based metrics. Bolded values are $p < 0.05$.

	p-values for univariate comparisons between times with and without detected seismic pulses	
Metric	***t*-test**	**Permutation test**
SPL	$\mathbf{9.8 \times 10^{-37}}$	$\mathbf{<1 \times 10^{-4}}$
SVL	$\mathbf{6.3 \times 10^{-32}}$	$\mathbf{<1 \times 10^{-4}}$
SPL_{pk}	$\mathbf{5.7 \times 10^{-41}}$	$\mathbf{<1 \times 10^{-4}}$
SVL_{pk}	$\mathbf{2.9 \times 10^{-24}}$	$\mathbf{<1 \times 10^{-4}}$
Kurtosis	$\mathbf{1.7 \times 10^{-8}}$	$\mathbf{<1 \times 10^{-4}}$
$Kurtosis_v$	2.0×10^{-1}	0.36
CF	$\mathbf{1.9 \times 10^{-38}}$	$\mathbf{<1 \times 10^{-4}}$
CF_v	$\mathbf{3.7 \times 10^{-9}}$	$\mathbf{<1 \times 10^{-4}}$
ACI	$\mathbf{1.8 \times 10^{-13}}$	$\mathbf{<1 \times 10^{-4}}$
ACI_v	$\mathbf{6.8 \times 10^{-7}}$	0.058

Therefore, any inferences on particle velocity levels, particularly in the context of bioacoustics studies, must strongly consider biases due to flow noise.

D. Relationships between pressure and particle velocity metrics

In the free field, away from any reflecting boundaries, particle velocity can be directly inferred from acoustic pressure by scaling the pressure by the acoustic impedance of sea water. Since this relationship can be complicated (but not unquantifiable) (Dahl *et al.*, 2024) near reflecting boundaries, an effort was made to discern the relationship between each of the discussed particle velocity and pressure metrics. Peak sound pressure, sound pressure level, sound exposure level, and CF for acoustic pressure and particle velocity were compared in the same unit space by reporting the velocity metrics in dB re 1 μPa by dividing the velocity metric value by ρ_0*c (Fig. 9). Throughout the data series, SPL and SVL are well correlated with 51% of the variance in SVL described by SPL. SEL and SEL_v were also well correlated, both in minute and hourly minute intervals ($R^2 = 0.697$ and 0.487 for 1 and 60 min intervals, respectively) (Table II; Fig. 9). SPL_{pk} and SVL_{pk} are less tightly correlated, but still show a significant correlation (Fig. 9; Table II). The higher order metrics (CF, ACI, and kurtosis) had much weaker correlations over the entire time series

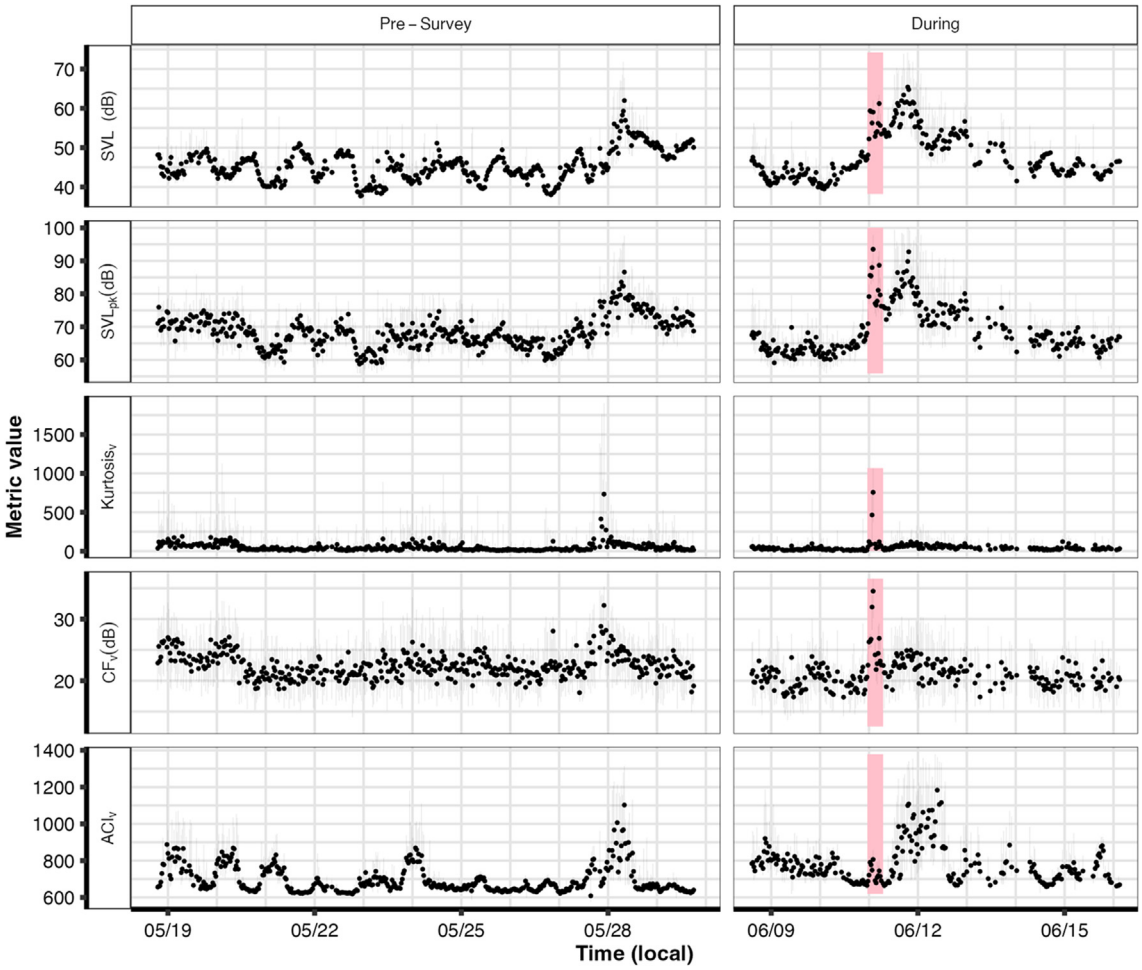

FIG. 7. Time series of soundscape metrics for the particle velocity magnitude for the sensor 35 cm above sea floor (bandpass filtered 50–3000 Hz). Metrics were calculated for every minute of data after removing times of detected flow noise contamination, each marker is median of 30 min, with the 20th to 80th percentiles of data shown in bars. "Post-survey" data are excluded as they were heavily influenced by flow noise. Within the displayed times, we have removed markers corresponding to periods with greater than 80% of the time suspect to flow noise as the remaining time was not likely to be representative. Time period where seismic pulses were detected are highlighted in the during period.

https://doi.org/10.1121/10.0036728

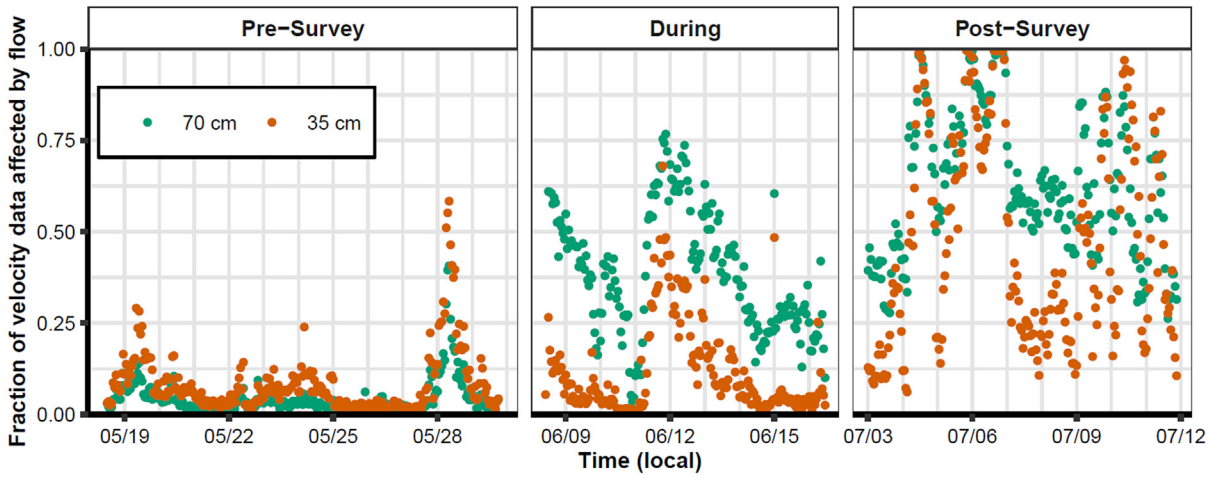

FIG. 8. Time series of times affected by flow noise, binned for each 60 min of data.

($R^2 < 0.1$), suggesting these metrics in pressure vs velocity present a more complex and less predictive relationship (Fig. 9; Table II).

When filtered only for periods when seismic pulses were present (Fig. 10), a stronger correlation is observed between all pressure and velocity metrics, suggesting that high signal-to-noise ratio (SNR) sound from distinct, time-limited sources have a tighter pressure-particle velocity relationship, while the relationship is less pronounced for diffuse ambient sound. Apart from ACI, over 70% of variance in the velocity metrics were described by its associated pressure metric ($R^2 > 0.7$ for each pair of metrics, Table II). This finding is consistent with those by Flamant and Bonnel (2023) and Dahl *et al.*, (2024). Note that to explore these correlation relationships, we masked the data to only include time without flow noise (for both the velocity and pressure metrics), and it is possible this masking could produce biases against times or conditions that are the ultimate source of the flow noise.

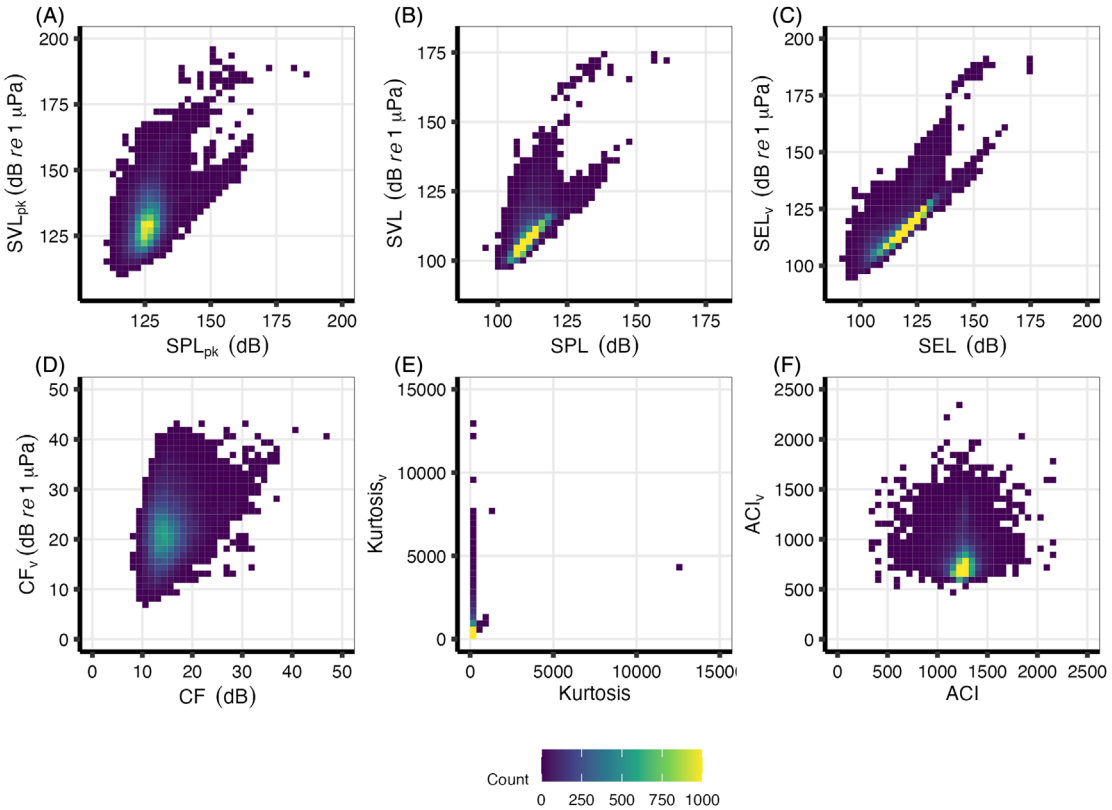

FIG. 9. Two-dimensional histogram of sound pressure and particle velocity metrics for the time series, all have been calculated excluding times affected by flow and the "post-survey" time period is excluded. Statistics for 1 min intervals for the 35 cm sensor are shown; note that velocity metrics (y axes) are shown in pressure equivalent units for comparison. Correlation coefficients are reported in Table II.

TABLE II. Summary statistics for Pearson correlation between pressure and velocity metrics, with 95% confidence interval obtained by bootstrapping. All correlations had a p-value of < 0.0001, as determined by random resampling. All metrics have been calculated excluding times affected by flow noise.

Variables	R^2	R^2 confidence interval (95%)
1 min metrics		
SPL_{pk} vs SVL_{pk}	0.255	0.243–0.269
SPL vs SVL	0.512	0.499–0.524
SEL vs SEL_v	0.697	0.689–0.705
CF vs CF_v	0.070	0.064–0.077
Kurtosis vs $kurtosis_v$	0.005	< 0.001–0.015
ACI vs ACI_v	< 0.001	< 0.001–0.002
1-min metrics; times with detected seismic pulses only		
SPL_{pk} vs SVL_{pk}	0.812	0.704–0.897
SPL vs SVL	0.861	0.807–0.903
SEL vs SEL_v	0.864	0.808–0.902
CF vs CF_v	0.716	0.506–0.863
Kurtosis vs $kurtosis_v$	0.758	0.411–0.926
ACI vs ACI_v	0.213	0.070–0.041
60-minute metrics		
SEL vs SEL_v	0.487	0.374–0.588

IV. CONCLUSIONS

In this study, acoustic pressure and particle motion was measured inside the RRMR in southern Oregon before, during, and after a nearby seismic airgun survey of the Cascadia Subduction Zone. The acoustic environment, when expressed in terms of pressure-based metrics, such as SPL, SPL_{pk}, CF, and ACI, was found to be dominated by mostly diel wind noise, with occasional contributions from seismic airgun pulses from the seismic surveys when the *R/V Langseth* was less than 50 km away and storm activity. The ambient noise floor appeared to scale with wind speeds, with the highest ambient noise levels occurring during the post-survey period. Particle velocity metrics were also sensitive to ambient noise, though they showed greater variability and less sensitivity to seismic airgun pulses.

Despite their potential for studying particle velocity, we found that vector sensors were significantly affected by flow noise, particularly during periods of high wind and wave action. After identifying and removing times with flow noise contamination, strong correlations between sound pressure (peak and RMS) and sound exposure level pressure and particle velocity metrics were observed–particularly during seismic pulses, suggesting that these two measurements are relatable when monitoring distinct sound sources with high signal to noise ratio. It has been shown recently that for time-averaged metrics, such as kinetic and potential energy and sound exposure levels (Dahl *et al.*, 2024), there is little value in separate measurements of particle velocity, which are considerably more challenging to make than pressure. Here, those conclusions are recapitulated using a different approach. While kinematic dosages can still be considered in terms of particle velocity, their exceedance (or not) can likely simply be considered in terms of their acoustic pressure equivalent.

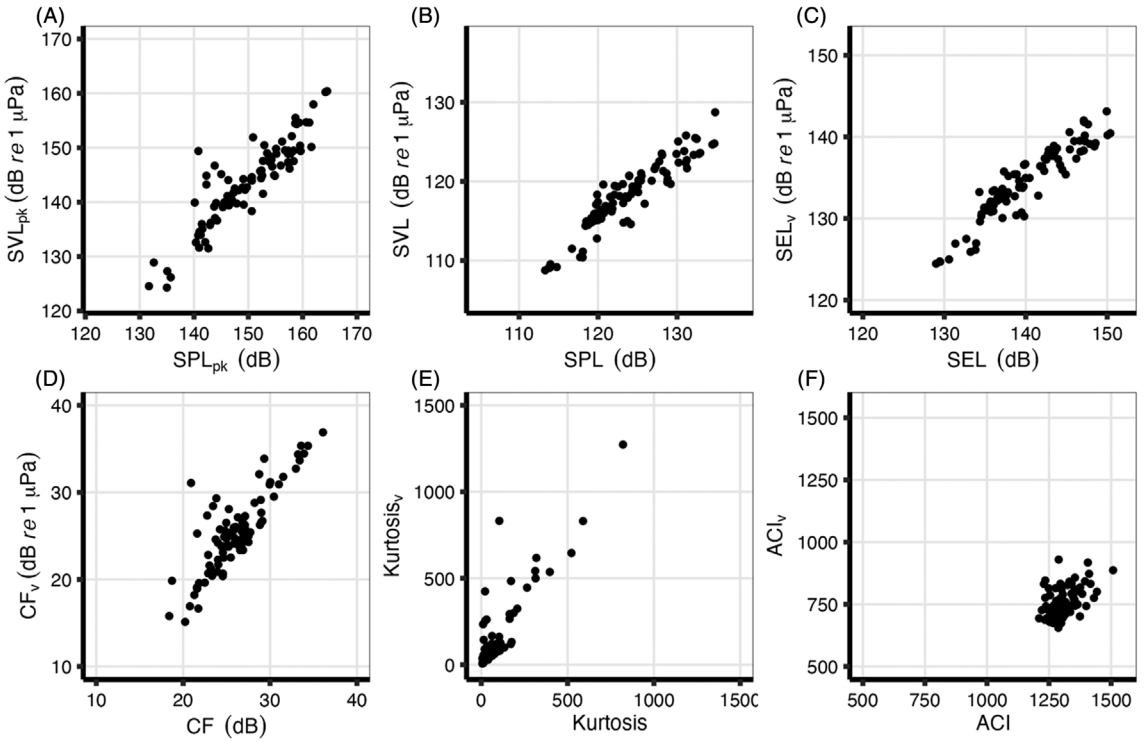

FIG. 10. Scatter plot of pressure and velocity metrics. Statistics for 1 min intervals for the 35 cm sensor are shown; subset for only those minutes with detected seismic pulses; all metrics have been calculated excluding times affected by flow. Note that velocity metrics (y axes) are shown in pressure equivalent units for comparison. Correlation coefficients are reported in Table II.

ACKNOWLEDGMENTS

Field data collection was supported by National Science Foundation (NSF) Grant No. 2118594 to Oregon State University with assistance from Oregon Sea Grant and the Bureau of Ocean Energy Management. Data analysis was supported by NSF Grant No. 2123682 to Oregon State University.

AUTHOR DECLARATIONS

Conflict of Interest

The authors have no conflicts to disclose.

DATA AVAILABILITY

Raw data were generated at the Integral Consulting Inc.'s facility. Derived data supporting the findings of this study are available from the corresponding author upon reasonable request.

Amante, C., and Eakins, B. W. (**2009**). "ETOPO1 arc-minute global relief model: procedures, data sources and analysis," available at https://repository.library.noaa.gov/view/noaa/1163.

Bohnenstiehl, D. R., Lyon, R. P., Caretti, O. N., Ricci, S. W., and Eggleston, D. B. (**2018**). "Investigating the utility of ecoacoustic metrics in marine soundscapes," J. Echoacoust. **2**, 1.

Bonnel, J., Flamant, J., Dall'Osto, D. R., Le Bihan, N., and Dahl, P. H. (**2021**). "Polarization of ocean acoustic normal modes," J. Acoust. Soc. Am. **150**, 1897–1911.

Carbotte, S. M., Boston, B., Han, S., Shuck, B., Beeson, J., Canales, J. P., Tobin, H., Miller, N., Nedimovic, M., Tréhu, A., Lee, M., Lucas, M. C., Jian, H., Jiang, D., Moser, L., Anderson, C., Judd, D., Fernandez, J., Campbell, C., Goswami, A., and Gahlawat, R. (**2024**). "Subducting plate structure and megathrust morphology from deep seismic imaging linked to earthquake rupture segmentation at Cascadia," Sci. Adv. **10**, eadl3198.

Casper, B. M., Smith, M. E., Halvorsen, M. B., Sun, H., Carlson, T. J., and Popper, A. N. (**2013**). "Effects of exposure to pile driving sounds on fish inner ear tissues," Comp. Biochem. Physiol. A. Mol. Integr. Physiol. **166**, 352–360.

Dahl, P. H., Bonnel, J., and Dall'Osto, D. R. (**2024**). "On the equivalence of scalar-pressure and vector-based acoustic dosage measures as derived from time-limited signal waveforms," J. Acoust. Soc. Am. **155**, 3291–3301.

Dahl, P. H., and Dall'Osto, D. R. (**2022**). "Potential and kinetic energy of underwater noise measured below a passing ship and response to sub-bottom layering," J. Acoust. Soc. Am. **152**, 3648–3658.

D'Spain, G. L., Hodgkiss, W. S., and Edmonds, G. L. (**1991**). "Energetics of the deep ocean's infrasonic sound field," J. Acoust. Soc. Am. **89**, 1134–1158.

Farina, A., and Morri, D. (**2008**). "Source-sink & ecofield: Ipotesi ed evidenze sperimentali. Proceedings SIEP-IALE Bari," Ecol. E Gov. Paesaggio ITA, 365–372, available at https://ora.uniurb.it/handle/11576/2299156.

Fay, R. R. (**1984**). "The Goldfish ear codes the axis of acoustic particle motion in three dimensions," Science **225**, 951–954.

Flamant, J., and Bonnel, J. (**2023**). "Broadband properties of potential and kinetic energies in an oceanic waveguide," J. Acoust. Soc. Am. **153**, 3012–3024.

Gordon, J., Gillespie, D., Potter, J., Frantzis, A., Simmonds, M. P., Swift, R., and Thompson, D. (**2003**). "A review of the effects of seismic surveys on marine mammals," Technol. Soc. J. **37**, 16–34.

Gray, M., Rogers, P. H., and Zeddies, D. G. (**2016**). "Acoustic particle motion measurement for bioacousticians: Principles and pitfalls," Proc. Mtgs. Acoust. 27, 010022.

Halvorsen, M. B., Casper, B. M., Matthews, F., Carlson, T. J., and Popper, A. N. (**2012**). "Effects of exposure to pile-driving sounds on the lake sturgeon, Nile tilapia and hogchoker," Proc. R. Soc. B **279**, 4705.

Haxel, J. H., Matsumoto, H., Meinig, C., Kalbach, G., Lau, T.-K., Dziak, R. P., and Stalin, S. (**2019**). "Ocean sound levels in the northeast Pacific recorded from an autonomous underwater glider," PLoS One **14**, e0225325.

Hothorn, T., Hornik, K., van de Wiel, M. A, and Zeileism A. (**2006**). "A Lego system for conditional inference," Am. Stat. **60**(3), 257–263.

Jones, I. T., D Gray, M., and Mooney, T. A. (**2022**). "Soundscapes as heard by invertebrates and fishes: Particle motion measurements on coral reefs," J. Acoust. Soc. Am. **152**, 399–415.

Martin, B. (**2013**). "Computing cumulative sound exposure levels from anthropogenic sources in large data sets," Proc. Mtgs. Acoust. **19**, 010048.

Mattmüller, R. M., Thomisch, K., Hoffman, J. I., and Van Opzeeland, I. (**2024**). "Characterizing offshore polar ocean soundscapes using ecoacoustic intensity and diversity metrics," R. Soc. Open Sci. **11**, 231917.

McArdle, B. H., and Anderson, M. J. (**2001**). "Fitting multivariate models to community data: A comment on distance-based redundancy analysis," Ecology **82**, 290–297.

McCauley, R., Fewtrell, J., Duncan, A., Jenner, C., Jenner, M.-N., Penrose, J., Prince, R., Adhitya, A., Murdoch, J., and McKabe, K. (**2003**). "Marine seismic surveys: Analysis and propagation of air-gun signals; and effects of exposure on humpback whales, sea turtles, fishes and squid," in *Environmental Implications of Offshore Oil and Gas Development in Australia: Further Research: A Compilation of Three Scientific Marine Studies* (Australian Petroleum Production and Exploration Association, Canberra, Australia), pp. 364–521, available at https://espace.curtin.edu.au/handle/20.500.11937/80319 (Last viewed May 13, 2025).

Mooney, T. A., Hanlon, R., Madsen, P. T., Christensen-Dalsgaard, J., Ketten, D. R., and Nachtigall, P. E. (**2012**). "Potential for sound sensitivity in cephalopods," in *The Effects of Noise on Aquatic Life, Advances in Experimental Medicine and Biology*, edited by A. N. Popper and A. Hawkins (Springer, New York), Vol. 730, pp. 125–128.

Nedelec, S. L., Campbell, J., Radford, A. N., Simpson, S. D., and Merchant, N. D. (**2016**). "Particle motion: The missing link in underwater acoustic ecology," Methods Ecol. Evol. **7**, 836–842.

Oksanen, J., Simpson, G., Blanchet, F., Kindt, R., Legendre, P., Minchin, P., O'Hara, R., Solymos, P., Stevens, M., Szoecs, E., Wagner, H., Barbour, M., Bedward, M., Bolker, B., Borcard, D., Borman, T., Carvalho, G., Chirico, M., De Caceres, M., Durand, S., Evangelista, H., FitzJohn, R., Friendly, M., Furneaux, B., Hannigan, G., Hill, M., Lahti, L., McGlinn, D., Ouellette, M., Ribeiro Cunha, E., Smith, T., Stier, A., Ter Braak, C., and Weedon, J. (**2025**). vegan: Community Ecology Package. R package version 2.7-0, available at https://vegandevs.github.io/vegan/.

Pante, E., and Simon-Bouhet, B. (**2013**). "marmap: a package for importing, plotting and analyzing bathymetric and topographic data in R," PLoS One **8**(9), e73051.

Pegg, N., Roca, I. T., Cholewiak, D., Davis, G. E., and Van Parijs, S. M. (**2021**). "Evaluating the efficacy of acoustic metrics for understanding baleen whale presence in the Western North Atlantic ocean," Front. Mar. Sci. **8**, 749802.

Pieretti, N., Farina, A., and Morri, D. (**2011**). "A new methodology to infer the singing activity of an avian community: The Acoustic Complexity Index (ACI)," Ecol. Indic. **11**, 868–873.

Popper, A. N., and Hawkins, A. D. (**2018**). "The importance of particle motion to fishes and invertebrates," J. Acoust. Soc. Am. **143**, 470–488.

Raghukumar, K., Chang, G., Spada, F., and Jones, C. (**2020**). "A vector sensor-based acoustic characterization system for marine renewable energy," J. Mar. Sci. Eng. **8**(3), 187.

Raghukumar, K., Chang, G., Spada, F., Jones, C., Spence, J., Griffin, S., and Roberts, J. D. (**2019**). "Performance characteristics of a vector sensor array in an energetic tidal channel," Sandia National Lab. (SNL-NM) (Sandia National Labs, Albuquerque, NM), available at https://www.osti.gov/servlets/purl/1641799 (Last viewed May 13, 2025).

Richardson, W. J., Würsig, B., and Greene, C. R., Jr. (**1986**). "Reactions of bowhead whales, *Balaena mysticetus*, to seismic exploration in the Canadian Beaufort Sea," J. Acoust. Soc. Am. **79**, 1117–1128.

Thode, A., Skinner, J., Scott, P., Roswell, J., Straley, J., and Folkert, K. (**2010**). "Tracking sperm whales with a towed acoustic vector sensor," J. Acoust. Soc. Am. **128**, 2681–2694.

Thode, A. M., Norman, R. G., Conrad, A. S., Tenorio-Hallé, L., Blackwell, S. B., and Kim, K. H. (**2021**). "Measurements of open-water arctic ocean noise directionality and transport velocity," J. Acoust. Soc. Am. **150**, 1954–1966.

Wilford, D. C., Miksis-Olds, J. L., Martin, S. B., Howard, D. R., Lowell, K., Lyons, A. P., and Smith, M. J. (**2021**). "Quantitative soundscape analysis to understand multidimensional features," Front. Mar. Sci. **8**, 672336.